ChemPubSoc Europe

DOI: 10.1002/celc.201600730

CHEMELECTROCHEM Communications

Lithium Deposition from a Piperidinium–based Ionic Liquid: Rapping Dendrites on the Knuckles

Claudia A. Berger,[a] Maximilian U. Ceblin,[a] and Timo Jacob*[a, b, c]

Using cyclic voltammetry (CV), *in-situ* scanning tunneling microscopy (STM) and electrochemical quartz crystal microbalance (EQCM) the initial stages of lithium deposition on Au(111) from a solution of lithium bis(trifluoromethylsulfonyl)imide in the commercially available ionic liquid 1-methyl-1-propylpiperidinium bis(trifluoromethylsulfonyl)imide (MPPipTFSI) were investigated. We could identify three distinct cathodic peaks in the potential range from 0 to −2.5 V (vs. Pt *quasi*-reference electrode), corresponding to different lithium deposition modes. While in the potential region of the under-potential deposition (UPD) (−1.2 to −1.8 V) the growth of monoatomic high islands (300–370 pm) takes place, Li bulk deposition occurs at potentials <-2.3 V. Finally, the third peak at 0 V, which only appears after a previous bulk deposition, is connected to a strand-like growth of lithium at (111) terraces with a uniform orientation over the whole substrate. Interestingly, once reaching a step-edge, the one-dimensional growth continues into the electrolyte, indicating the initial stages of Li dendrite formation.

Lithium ion batteries are key components for consumer electronics in many areas, such as portable, telecommunication and computing equipment, due to their high energy density, high voltage and light weight.[1,2] This makes them promising candidates for large-scale applications in hybrid and electric vehicles besides lithium sulfur and lithium air batteries, which contain lithium metal anodes.[3] However, the realization of higher capacity and safer systems is still hampered by a severe lack in a detailed understanding of the fundamental electrochemical processes, indicating the necessity for extensive and detailed studies to investigate and solve these problems. One important issue is connected to the growth of metallic Li-dendrites. The successive deposition and stripping of lithium, occurring during charge-discharge cycling, usually results in a dendritic morphology at high current densities.[4] These structures have the potential to grow through the cell, forming a metallic interconnect between positive and negative electrodes and finally causing an internal short circuit. This may finally cause severe safety hazards, due to the insufficient thermal stability of commonly used electrolytes and the associated danger of explosion.[5] Recent literature claims two different dendritic growth modes, the one-dimensional needle growth and a three-dimensional bush growth.[6,7] In both cases, the lithium filament growth is supposed to start at kinks by insertion. It was shown that the needle growth is an inherent tendency of the lithium metal and is not depending on the deposition technique or the composition of the surface electrolyte interface (SEI).[8] The three-dimensional bush growth is claimed to be controlled by the structure of the solid electrolyte interphase (SEI). Consequently, there are two main goals. Firstly, the reduction of the mobility of lithium ions, which could prevent the formation of dendritic precursors, or secondly, the influence of the SEI on further dendrite growth.[8] Extensive research regarding the effect of the electrolyte composition in order to suppress dendrite growth and to improve safety have been performed. Former literature is concerned with the application of polymer electrolytes, additives, electrolyte mixtures and few room- temperature ionic liquids.[5,9–14] As often the first atoms dictate the subsequent growth, in the present work we concentrated exactly on the structure and behavior of these first atoms, investigating the initial stages of lithium deposition and the growth of dendrites on well-defined model systems. Based on a detailed understanding of the growth one might deduce ideas to prevent the formation of dendritic precursors and their further growth. In lithium ion batteries mostly employed electrode materials are graphite and nanocrystalline amorphous silica. Here, lithium has the nature to migrate into the electrode material, for one thing via intercalation and for another thing via alloy formation. A feature which can be observed on Au as well, since a Li/Au-surface alloy is formed. Therefore, we believe Au single crystals are suitable model systems that allow for detailed investigations to understand the fundamental process of Li electrodeposition on the atomic scale, especially in contact with ionic liquids (ILs). ILs are organic salts and are thus consistent solely of ions. A vast number of possible combinations of different anions and cations is possible, which results in a large variety of different ILs. Further, they are defined to have melting points below 100 °C, and many of the ILs are in molten state even at room-temperature. These room-temperature ionic liquids (RTILs) are expected to be well-suited for the application as an electrolyte in electrochemistry due to their unique properties. They provide low vapor pressure and high thermal stability combined with large electrochemical windows and good ionic conductivities.[15–20] Besides these advantages, one should also

[a] *Dipl.-Chem. C. A. Berger, M. U. Ceblin, Prof. Dr. T. Jacob*
Institute of Electrochemistry, Ulm University, Albert-Einstein-Allee 47, 89081 Ulm, Germany
E-mail: timo.jacob@uni-ulm.de
[b] *Prof. Dr. T. Jacob*
Helmholtz-Institute Ulm (HIU) Electrochemical Energy Storage, 89081 Ulm, Germany
[c] *Prof. Dr. T. Jacob*
Karlsruhe Institute of Technology (KIT), P.O. Box 3640, 76021 Karlsruhe, Germany

Supporting information for this article is available on the WWW under http://dx.doi.org/10.1002/celc.201600730

mention unfavorable features, which are high viscosities and often high costs. Additionally, possible toxicities and ecologically-damaging impacts, respectively, are not yet fully understood and often underestimated. Nevertheless, RTILs grant the desired features of electrochemical and thermal stability for battery applications, making them promising candidates for next-generation battery electrolytes. Previous studies have shown that specific RTILs are able to form a solid electrolyte interphase (SEI), which is comparable to carbonate-based electrolytes.[21] Although, RTILs usually allow for only 10–100 cycles, which is below the usual cyclability of 500–1000 cycles for standard electrolytes, in principle they posses all attributes required for application in batteries. Even more interesting, they can be used as electrolytes for electrochemical model investigations of the initial stages of metal deposition. Therefore, they are interesting systems for detailed studies of lithium deposition and dendrite growth, where the yielded results can be transferred to lithium ion batteries, as well as lithium sulfur and lithium air batteries.

Figure 1 shows the first and the second cycle of the cyclic voltammogram (CV) of 0.02 mol/L LiTFSI/MPPipTFSI on Au(111),

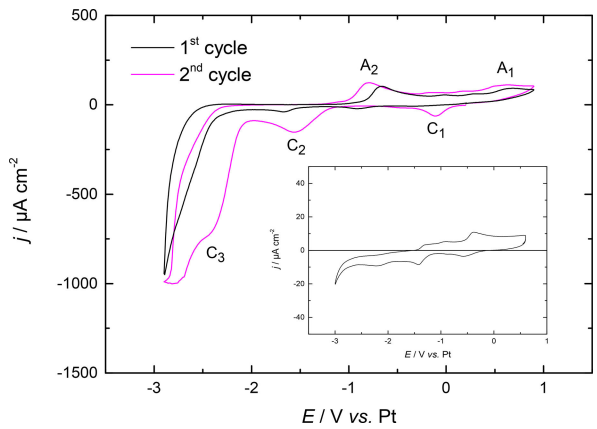

Figure 1. First two CV cycles of 0.02 mol/L LiNTFSI + MPPipTFSI on Au(111) at a scan rate of 50 mV/s. Inset: CV (50 mV/s) of pure MPPipTFSI on Au(111).

recorded with a scan rate of 50 mV/s. The CV with the same scan rate of 50 mV/s of the pure RTIL on Au(111) is given in the inset. It shows a flat, double-layer-type behavior over a large potential range from −3.0 to +0.6 V, however some small humps appear, which seem to be due to adsorption processes of the composing ions on the electrode surface, rearrangements of the gold surface or minor impurities.

The potential where the irreversible decomposition of the ions of the electrolyte takes place is beyond the potential range of the CV, visible at the low current densities at the reversal potentials. Regarding the CV after adding LiTFSI, one can notice three cathodic peaks C_1, C_2 and C_3 at potentials of 0 V, −1.4 V and −2.3 *vs.* Pt, where peak C_1 does not show up in the first cycle, but appears once the system has been once exposed to potentials < -1.4 V accompanied by high current densities. C_2 can be identified as the UPD peak of lithium.[22] The corresponding cathodic charge of about 500 µC/cm^2, as derived from the CV in Figure 1 is equivalent to the overall deposition of around two monolayers of Li, the structure that will be discussed later. This is in good agreement with the hitherto published results.[22,23] Peak C_3 indicates the bulk deposition of Li.[5,24–27] As already mentioned before, peak C_1 is not present in the first cycle of the CV, but in all following cycles once a potential in the lithium UPD region is applied (−1.4 V), increasing with the number of cycles. The charge determined from peak C_1 in the second CV cycle amounts to 180 µC/cm^2. Based on the CV measurements alone, one cannot clearly distinguish whether peak C_1 is caused either by Au, e.g. lifting of the surface reconstruction, or by processes related to Li. In the reverse scan the anodic peaks A_1 and A_2 can be related to the oxidation of lithium. In previous studies the reduction of lithium is reported to proceed in different growth modes, which means the growth of islands right up to the formation of two monolayers and also the formation of an Au/Li surface alloy in several phases with up to 39% Li, replacing Au in the fcc structure.[22,23,28] Hence, it is hardly surprising to find several oxidation peaks for lithium. Subsequent window opening experiments (see ESI) indicated that peak A_1 seems to be correlated to the UPD peak C_2. Further, the window opening experiments showed that the anodic peak A_2 seems to be related to the lithium bulk deposition C_3. Comparing the charges of these peaks indicates that these processes are not fully reversible, instead we observe an amount of 10% of deposited lithium, which is dissolving again, according to the changes in the CV peak areas. Of course, it cannot be fully excluded that the oxidation of specific lithium phases may proceed at potentials beyond the positive limit of the stability range of the IL (>0.8 V) and are thus not apparent in the shown CV. The presence of lithium adspecies in an amount exceeding a monolayer on the Au substrate after electrodeposition was approved by x-ray photoelectron spectroscopy (see ESI).

Figure 2(b) is recorded at −2.3 V, i.e. in the region of peak C_3 in the Figure 2(a) shows an *in-situ* scanning tunneling

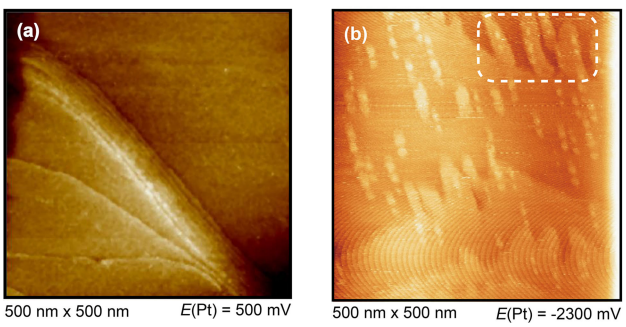

Figure 2. *In-situ* STM images of LiTFSI/MPPipTFSI on Au(111) at different electrode potentials.

microscopy (STM) image of the free Au surface at 0.5 V *vs.* Pt. CV. At these low potentials, lithium bulk deposition occurs in a three-dimensional growing mode. This becomes particularly visible in the marked area of Figure 2(b).

Here it can be noticed that there are large islands with a width of 30–40 nm and a length of 130–170 nm, where the growth seems to initiate from Au step edges. On top of these islands, the additional formation of smaller islands with a diameter around 10 nm can be observed. The corresponding height profiles indicate a height of 300–350 pm per layer, which indicates a possible deposition of lithium. In the intermediate potential region, which means around −1.4 V, the STM image shown in Figure 3 was obtained. Here the beginning of island

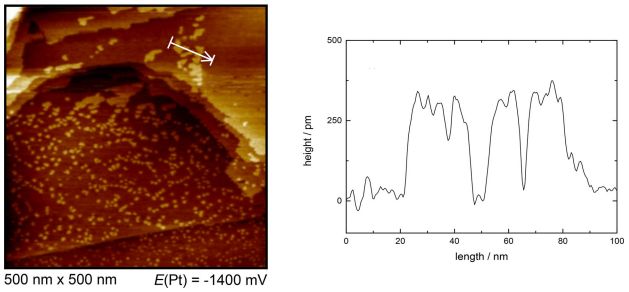

Figure 3. *In-situ* STM image of LiTFSI/MPPipTFSI on Au(111) at −1.4 V with related height profile.

deposition of lithium can be observed, showing islands of one monolayer height. Along the progressing scan, i.e. elapsing time, the growth of these islands can be observed. The scan direction in Figure 3(b) proceeds vertically from the bottom to the top of the STM image. At the beginning of the scan the diameter of the island is less than 10 nm (bottom), while their size amounts to 20–30 nm at the end of the scan (top). According to the height profile along the arrow highlighted in the STM image of Figure 3, the average height of the deposited islands amounts to around 300 pm, which is in the magnitude of elemental lithium.

The STM images shown in Figure 4 are recorded at a potential of 0 V, which corresponds to the potential regime of

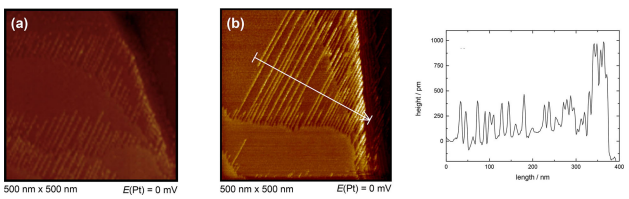

Figure 4. *In-situ* STM image of LiTFSI/MPPipTFSI on Au(111) at 0 V (a) after 10 min and (b) after 40 min with related height profile (indicated by an arrow).

peak C_1 in the CV. In general, one can notice a strand-like growth of parallel rows, which could be an indication for the formation of dendritic lithium structures. Also remarkable is the uniform orientation over the complete substrate surface, where a growth following the symmetrically equivalent three spatial directions of the (111)-substrate can be excluded. Figure 4(a) shows the electrode surface after 10 minutes, where the dendritic structures already have an average length of 80–100 nm. The growth of these strands starts at a step edge and primarily proceeds growing parallel to the Au terrace. The average width of a strand amounts to 10 nm, what shows that a strand must be an agglomeration of several atoms along the horizontal axis. Also remarkable is the indication of a minimal distance between the strands, which is less than 5 nm, becoming especially visible at the tip of the arrow (see Figure 4(b)). Since this distance is approximately in the dimension of the cation size of the RTIL, the morphology of the deposit could be influenced by the adsorbate structures of the cations. The influence of cations on the metal deposition process has also been investigated and reported for other systems such as the deposition of aluminum and tantalum from various RTILs, for instance.[30] Figure 4(b) is recorded after 40 minutes at 0 V *vs.* Pt. Here many strands with uniform direction are observable, possessing an average length of >350 nm. Further, at the end of the terrace, there is a substrate subsidence of ca. 10 MLs. Here, the dendrite-like structures bends out of the substrate plane, starting to grow into the electrolyte. In the STM images this can be seen by the lighter shade at the end of the strands. The corresponding height profile along the arrow (see STM-image of Figure 4(b)) shows a height of these structures in the order of lithium on the terrace. Whereby an increase of the height to 1000 pm is apparent in the region of the subsidence (i.e. step edge) of the substrate. This also supports the previous conclusion of the dendritic behavior of the studied deposit, hence dendrites have the tendency to grow uniformly in one direction.[5] The investigated behavior very likely resembles the initial stages of dendrite growth into the electrolyte. In good accordance with our CV measurements is the observation that these images were obtained after exposing the system to potentials where lithium reduction takes place, which is also accompanied by high current densities. We assume that the previous formation of the precursor at negative potentials, namely the Li/Au surface alloy, is required for the formation of these dendritic structures at more positive potentials. To further quantify the deposition *in-situ* electrochemical quartz-crystal microbalance (EQCM) measurements combined with chronoamperometry were performed. Here, we can definitely exclude a possible deposition of heavy elements, such as Pt, which could arise from the counter electrode due to the high sensitivity of this method. Nevertheless, lithium is difficult to detect in small amounts due to its light weight. Therefore, the deposition was studied over longer time periods, resulting in overall masses that could be detected accurately. The EQCM results are shown in Figure 5(a)

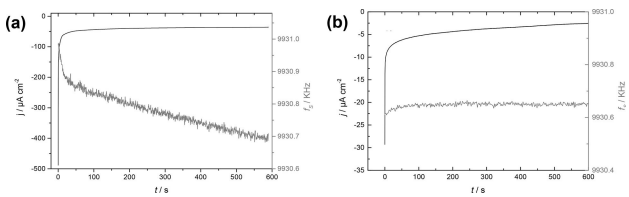

Figure 5. *In-situ* EQCM combined with chronoamperometry of LiTFSI/MPPipTFSI on Au at (a) −2.3 V and (b) 0 V *vs.* Pt.

for the bulk deposition region and Figure 5(b) for the dendrite formation region. In these figures the chronoamperometric measurement is plotted on the left hand side and the related EQCM frequency *vs.* time on the right hand side. In order to evaluate the deposited mass, we used the Sauerbrey equation

$$\Delta f_m = \frac{-2f_0^2}{A\left(\mu_q \rho_q\right)^{\frac{1}{2}}} \Delta m, \quad (1)$$

where Δf_m is the change in frequency resulting from the mass deposit Δm.[30] f_0 is the resonance frequency of the unloaded quartz crystal, A the surface area onto which deposition can occur and μ_q and ρ_q are the shear modulus and the density of the quartz, which can be combined into a constant C. Combining the Sauerbrey equation with Faraday's law the following expression is obtained

$$\frac{M}{z} = \frac{-\Delta f}{Q} C, \quad (2)$$

where M is the molar mass of the deposit, z is the number of exchanged electrons per ion and Q the charge related to the observed electrochemical process. Using equation (2), we determined the molecular mass of the deposit according to the resonance frequency change of the quartz crystal and the transferred charge during this process derived from the current-time transient. For the bulk deposition we obtain a mass around 6.4 g/mol, which is in good agreement with the molecular mass of lithium. Interestingly, in the region of the investigated dendritic growth (around 0 V *vs.* Pt) no change in the resonance frequency could be observed. Therefore we assume, that no significant increase in the mass on the surface took place. This also leads to the implication that the dendritic structures might result from the rearrangement of a potential Au/Li surface alloy formed during Li bulk deposition.

Using a combination of CV, *in-situ* STM and *in-situ* EQCM, we investigated the initial stages of lithium deposition from MPPipTFSI on Au(111) and could reveal three different deposition modes. We were able to record an STM image related to each cathodic peak in the CV. In the potential range of the second cathodic peak ($E_{Pt} = -1.4$ V) the growth of lithium islands of one monolayer height on the terraces as well as along the step edges could be observed. The third peak at very negative potentials ($E_{Pt} = -2.3$ V) coincides with the three-dimensional bulk deposition of lithium. After successive cycling of the potential, where high current densities appeared in the very negative potential region, we investigated a dendritic growth of lithium parallel to the gold terraces in the potential regime of the first cathodic peak ($E_{Pt} = 0$ V), leading to strand-like structures. Further, these lithium strands are aligned in solely one direction over the whole substrate surface and start bending out of the substrate plane once a subsidence is reached, representing the initial formation and growth of dendrites into the electrolyte. EQCM measurements clearly showed the deposition of lithium from the solution in the bulk deposition region. However, in the dendrite formation region, no significant mass increase on the surface could be observed, leading to the assumption that the dendritic structures most likely result from a rearrangement of the previously formed Au/Li surface alloy. In summary, the initial stages of Li deposition and dendrite growth could be observed for the first time. As dendrites do represent a severe safety issue in Li-ion batteries, our results provide important implications on how dendrites grow on the surface and finally into the electrolyte once a subsidence (e.g. step edge) is reached. Consequently, restricting the active potential range ($E_{Pt} > -2.3$ V) in order to avoid Li/Au alloy formation accompanying Li bulk deposition, might be the key to prevent from the precursor of dendritic lithium growth.

Experimental Section

1-methyl-1-propylpiperidinium bis(trifluoromethylsulfonyl)imide (MPPipTFSI) was purchased from IoLiTec (>99%). The ionic liquid was vacuum-dried for 24 h at elevated temperatures (80 °C) before adding the precursor lithium bis(trifluoromethylsulfonyl)imide (LiTFSI) in a concentration of 0.02 mol/L for the metal deposition. All experiments, including handling and storage of the used substances, were performed inside a glove box under argon atmosphere. Electrochemical investigations were carried out in self-designed cells made of KelF, each one with a volume of 150 µL, and a Au(111) single crystal (MaTeck GmbH, Juelich, FRG) with 12 mm diameter acting as working electrode. As stable counter and *quasi*-reference electrodes Pt wires (MaTeck GmbH, Juelich, FRG) were used, as Pt could not have been detected on the electrode surface by XPS measurements after electrochemical experiments (see ESI); thus, all potentials are given against the Pt reference. Prior to the measurements all electrodes were annealed in a hydrogen flame and cooled down slowly in an argon stream. All CVs were recorded with a Zahner IM6 potentiostat from Zahner Elektrik controlled by the Thales Z 1.20 USB software. Electrochemical *in-situ* STM studies were performed with a Veeco MultiMode8 Scanning Probe Microscope combined with a Nanoscope 5 Controller and a Bruker Universal Bipotentiostat. For the preparation of the STM tips, Pt/Ir wires (80:20) were electrochemically etched in 3.5 M NaCN and coated with BASF electrophoretic paint (ZQ84- 3225) to reduce the faradaic current. All images were recorded in the constant-current mode with a tip current between 1–3 nA. The experimental setup for the EQCM measurements is composed of a eQCM 10 M controller from Gamry Instruments and a HEKA 590 potentiostat. The used AT-cut quartz crystal (ICM International Crystal Manufacturing) contains a nominal resonance frequency of 10 MHz and is coated by circular poly-crystalline Au on both sides with 100 nm thickness and 0.235 cm^2 geometric surface area.

Conflict of Interest

The authors declare no conflict of interest.

Keywords: lithium · dendrites · ionic liquids · electrodeposition

[1] J. M. Tarascon, M. Armand, *Nature*, **2001**, *414*, 359–367.
[2] C. Liu, F. Li, L.-P. Ma, H.-M. Cheng, *Adv. Mater.*, **2010**, *22*, E28-E62.
[3] M. Ishikawa, T. Sugimoto, M. Kikuta, E. Ishiko, M. Kono, *J. Power Sources*, **2006**, *162*, 658–662.
[4] I. Yoshimatsu, T. Hirai, J.-I. Yamaki, *J. Electrochem. Soc.*, **1988**, *135*, 2422–2427.

[5] P. C. Howlett, D. R. MacFarlane, A. F. Hollenkamp, *Electrochem. Solid-State Lett.*, **2004**, *7*, A97–A101.
[6] J. Steiger, D. Kramer, R. Mönig, *J. Power Sources*, **2014**, *261*, 112–119.
[7] J. Steiger, D. Kramer, R. Mönig, *Electrochim. Acta*, **2014**, *136*, 529–536.
[8] J. Steiger, G. Richter, M. Wenk, D. Kramer, R. Mönig, *Electrochem. Comm.*, **2015**, *50*, 11–14.
[9] J. Y. Song, Y. Y. Wang, C. C. Wan, *J. Power Sources*, **1999**, *77*, 183–197.
[10] G. Appetecchi, F. Alessandrini, R. Duan, A. Arzu, S. Passerini, *J. Power Sources*, **2001**, *101*, 42–46.
[11] R. Mogi, M. Inaba, S.-K. Jeong, Y. Iriyama, T. Abe, Z. Ogumi, *J. Electrochem. Soc.*, **2002**, *149*, A1578–A1583.
[12] S. S. Zhang, *J. Power Sources*, **2006**, *162*, 1379–1394.
[13] O. Crowther, A. C. West, *J. Electrochem. Soc.*, **2008**, *155*, A806–A811.
[14] R.-S. Kühnel, N. Böckenfeld, S. Passerini, M. Winter, A. Balducci, *Electrochim. Acta*, **2011**, *56*, 4092–4099.
[15] F. Endres, *ChemPhysChem*, **2002**, *3*, 144–154.
[16] R. D. Rogers, K. R. Seddon, *Science*, **2003**, *302*, 792–793.
[17] M. J. Earle, J. M. S. S. Esperanca, M. A. Gilea, J. N. Canongia Lopes, L. P. N. Rebelo, J. W. Magee, K. R. Seddon, J. A. Widegren, *Nature*, **2006**, *439*, 831–834.
[18] F. Endres, S. Zein El Abedin, *Phys. Chem. Chem. Phys.*, **2006**, *8*, 2101–2116.
[19] H. Ohno in *Electrodeposition from Ionic Liquids, Vol. 1* (Eds.: F. Endres, D. MacFarlane, A. Abbott), WILEY-VCH, Weinheim, **2008**, pp. 47–82.
[20] M. Freemantle, An introduction to Ionic Liquids , *Vol. 1*, RSC Publishing, Cambridge, **2009**, pp. 31–39.
[21] A. Lewandowski, A. Świderska-Mocek, *J. Power Sources*, **2009**, *194*, 601–609.
[22] L. H. S. Gasparotto, N. Borisenko, N. Bocchi, S. Zein El Abedin, F. Endres, *Phys. Chem. Chem. Phys.*, **2009**, *11*, 11140–11145.
[23] Y. Mo, Y. Gofer, E. Hwang, Z. Wang, D. A. Scherson, *J. Electroanal. Chem.*, **1996**, *409*, 87–93.
[24] B. J. Piersma, D. M. Ryan, E. R. Schumacher, T. L. Riechel, *J. Electrochem. Soc.*, **1996**, *143*, 908–913.
[25] Y. Fung, R. Zhou, *J. Power Sources*, **1999**, *81–82*, 891–895.
[26] H. Matsumoto, H. Sakaebe, K. Tatsumi, *J. Power Sources*, **2005**, *146*, 45–50.
[27] K. Tsunashima, M. Sugiya, *Electrochem. Solid-State Lett.*, **2008**, *11*, A17–A19.
[28] F. Renner, H. Kageyama, Z. Siroma, M. Shikano, S. Schöder, Y. Gründer, O. Sakata, *Electrochim. Acta*, **2008**, *53*, 6064–6069.
[29] F. Endres, O. Hofft, N. Borisenko, L. H. Gasparotto, A. Prowald, R. Al-Salman, T. Carstens, R. Atkin, A. Bund, S. Zein El-Abedin, *Phys. Chem. Chem. Phys.*, **2010**, *12*, 1724–1732.
[30] G. Sauerbrey, *Z. Phys.*, **1959**, *155*, 206.

Manuscript received: November 19, 2016
Accepted Article published: November 29, 2016
Final Article published: December 20, 2016